

pubs.acs.org/JPCA Article

Anion Photoelectron Imaging Spectroscopy of $C_6HF_5^-$, $C_6F_6^-$, and the Absence of $C_6H_2F_4^-$

Conor J. McGee, Kristen Rose McGinnis, and Caroline Chick Jarrold*



Cite This: J. Phys. Chem. A 2023, 127, 8556-8565



Read Online

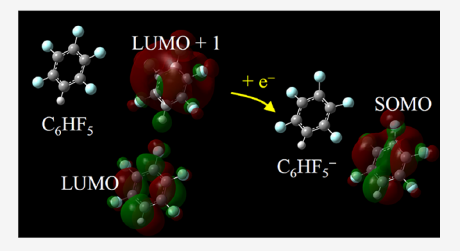
ACCESS I

III Metrics & More

Article Recommendations

SI Supporting Information

ABSTRACT: Substituents have a profound effect on the electronic structure of the benzene molecule. In this paper, we present new photoelectron spectra of the $C_5HF_5^-$ molecular anion, to test predictions [Int. J. Quant. Chem. **2017**, 188, e25504] that pentafluorobenzene has a positive electron affinity, as hexafluorobenzene was already known to have. The PE spectrum of $C_6HF_5^-$ exhibits a broad and vibrationally unresolved band due to significant differences between the structure of the anion and the neutral. The vertical detachment energy (VDE) of $C_5HF_5^-$ is determined to be 1.33 \pm 0.05 eV, and the lowest binding energy at which the signal is observed is 0.53 \pm 0.05 eV, which, if taken as the electron affinity, is in good agreement with the computed value. In



addition, we attempted to generate intact $C_6H_2F_4^-$ molecular ions using the 1,2,3,4-tetrafluorobenzene, 1,2,3,5-tetrafluorobenzene, and 1,2,4,5-tetrafluorobenzene precursors, as tetrafluorobenzene was predicted to have a near-zero but marginally positive electron affinity. Using a photoemission anion source, we were not able to produce the intact tetrafluorobenzene anion. Density functional theory calculations support a more detailed discussion of the impact of fluorine substitution on the electronic structure of these species.

1. INTRODUCTION

The electron affinities (EAs) of small, closed-shell hydrocarbons are typically negative, meaning their associated gasphase anions are metastable, or "temporary." The energies of these temporary anions relative to the neutral + free electron can be determined in several ways. Examples include electron transmission spectroscopy, $^{2-7}$ extrapolation of the EAs of solvated anions as the number of solvent molecules is decreased, e.g., $\mathrm{Nph}^-(\mathrm{H_2O})_x$ ($\mathrm{Nph}=\mathrm{naphthalene}$), and photodetachment spectroscopy of anion-molecule complexes in which the molecule carrying the excess charge serves as a proximal electron source for probing the neutral partner. $^{9-17}$

Certain functionalized, closed-shell organic molecules can form stable negative ions. Molecules with electron-withdrawing carbonyl groups such as glyoxal and related molecules are a case in point. In addition, larger molecules such as polycyclic aromatic hydrocarbons (PAHs) have long been known to have positive EAs, which increase with the size of the molecule. Whereas benzene and Nph both have negative EAs ($-1.1~{\rm eV}^2$ and $-0.20~{\rm eV},^8$ respectively), tricyclic 24,25 and larger PAH species $^{26-28}$ have positive EAs, with an increase on the order of tenths of eV with the number of rings.

An interesting opportunity arises in small stable molecules that have a range of identical functionalizable carbon centers, such as benzene, which open the door to systematically changing the EA of the molecule by varying the number of electron-withdrawing substituents. A previous density functional theory (DFT) study on F-substituted (and BO₂-substituted) benzene reported by Driver and Jena²⁹ predicted a crossover from negative to positive EA in the $C_6H_{6-x}F_x$ (0 \leq

 $x \leq 6$) series, where penta- and hexafluorobenzene were predicted to have definitively positive EAs; the EA of tetrafluorobenzene was predicted to be near zero; and the less fluorinated species were predicted to have definitively negative EAs. Experimentally, the hexafluorobenzene molecule has been shown to form both valence^{30–33} and nonvalence-bound anions, ^{31,34,35} both studied by anion photoelectron (PE) spectroscopy, but to our knowledge, evidence of the pentafluorobenzene anion has only been reported in past thermodynamic studies. ³⁶

In a related study, our group developed the technique noted above of probing temporary anions of "X" molecules having EA < 0, using photoedetachment of $O_2^-\cdot X$ anion—molecule complexes.⁹ This technique is akin to electron transmission spectroscopy in that the O_2^- anion serves as a point source of electrons that, upon photodetachment of O_2^- , can interact with the proximal X molecule. The temporary anion state energies of $X = C_6 H_{6-x} F_x$ ($0 \le x \le 4$), specifically, were reflected in high-intensity, broad resonances observed in the continuum electron kinetic energy (e⁻KE) distribution generated by detaching $O_2^-\cdot X$.

Received: June 14, 2023 Revised: September 18, 2023 Published: October 10, 2023





The utility of this approach in determining the energies of temporary excited states of anions with positive EA [e.g., $C_6H_{6-x}F_x$ (x = 5, 6)] comes into question for several reasons, one of which is the potential for these fluorobenzenes, rather than the O₂ partner molecule, to bind the electron.³⁷ Curiously, while C_6HF_5 was predicted to have a positive EA comparable to O_2 , 29,37 the PE spectrum of $[O_2 \cdot C_6HF_5]^$ resembled that of a typical anion-molecule complex: The spectrum was consistent with the charge being primarily carried by O₂⁻, yielding a spectral profile similar to O₂⁻, but solvent-shifted to higher electron binding energy (e-BE).9 In a previous study reported by our group, 21 bimolecular complex anions in which both molecules have competing EAs have PE spectra that deviate significantly from typical anion-molecule complex PE spectra. The PE spectrum of the $[O_2 \cdot O_2]^-$ anion is a well-known example. Similarly, the PE spectrum of the $[O_2 \cdot C_6 F_6]^-$ complex anion deviated from that of a simple O_2^- . **X** anion—molecule complex. Therefore, the $[O_2 \cdot C_6 HF_5]^-$ PE spectrum called into question whether C₆HF₅ indeed has a robust, positive EA comparable to O2 as predicted by Driver and Jena.29

To demonstrate whether and by what energy C_6HF_5 and $C_6H_2F_4$ bind an electron to form stable anions, we present the PE spectrum of $C_6HF_5^-$, along with the PE spectrum of $C_6F_6^-$ obtained using the same experimental setup for direct comparison with previously obtained $C_6F_6^-$ PE spectra. An analysis of photoelectron angular distributions (PADs) is also presented. As the PE spectrum of $C_6HF_5^-$ has not previously been reported, this provides the first experimental determination of the vertical detachment energy (VDE) and an upper limit on the adiabatic EA. A more accurate determination of the EA is complicated by the broad and vibrationally unresolved appearance of the spectrum, making the identification of the origin of the detachment transition difficult.

We also report our attempts to generate the tetrafluor-obenzene anion: Our inability to do so is consistent with the negative EA predicted by Davis et al. (-0.17 to -0.36 eV), depending on the specific coupled-cluster method).³⁷ However, Driver and Jena calculated a small but positive EA of +0.01 eV for the 1,2,3,5-tetrafluorobenzene isomer.²⁹ Computational results presented here predicted an EA of 0.004 eV for the same isomer, an EA of 0.13 eV for 1,2,3,4-tetrafluor-obenzene, and a negative EA for the 1,2,4,5-tetrafluorobenzene isomer. Mass spectra of anions generated from all three constitutional isomers of $C_6H_2F_4$ in the ion source used to successfully generate $C_6HF_5^-$ and $C_6F_6^-$ show the production of tetrafluorophenide, $C_6HF_4^-$, along with other fragment anions.

Finally, DFT calculations support a deeper exploration of the electronic structure of fluorine-substituted benzenes. In particular, trends of the relative stability of the unoccupied C– F σ^* molecular orbitals with F-substitution can be related to whether the EAs of these species are positive or negative.

2. METHODS

2.1. Experimental Details. The anion PE imaging apparatus used to generate the anions and probe them via photodetachment has been described elsewhere. Briefly, ions were generated by flowing a gas mixture of $C_6H_{6-x}F_x$ ($4 \le x \le 6$) [C_6F_6 from Santa Cruz Biotechnology, 98% purity; C_6HF_5 from Sigma-Aldrich, 98% purity, 1,2,4,5-tetrafluorobenzene from Santa Cruz Biotechnology, 98% purity; 1,2,3,5- and 1,2,3,4-tetrafluorobenzene from AmBeed, 99.6% and 98%

purity, respectively seeded in ultrahigh purity He and expanded using a pulsed molecular beam valve, operated at a 30 Hz repetition rate, into a photoemission source.³³ The source coupled the beam valve with a channel in which a Gd₂O₃ photoemitter surface was exposed. The attenuated (between 0.5 and 1 mJ/pulse) second harmonic output of a pulsed Nd:YAG laser (532 nm, 2.330 eV) was timed to impinge on the Gd₂O₃ surface in coincidence with the gas mixture flowing over it, resulting in the production of low kinetic energy electrons that can attach to species with positive EA. Outputs greater than 1.5 mJ/pulse result in significant molecular fragment ion formation. The nascent anions were thermalized in a 10 mm long, 3 mm diameter channel before expanding into the vacuum chamber. The ions are accelerated into a 0.97 m Bakker-style 44,45 beam-modulated time-of-flight mass spectrometer and, after passing through a mass defining slit, enter a detector region and collide with a dual microchannel plate ion detector. Ion flight times are recorded on a digitizing oscilloscope. The resolution of the mass spectrometer depends on the specific settings used, but typical $m/\Delta m$ values range between 150 and 300.

As no intact $C_6H_2F_4^-$ anions were generated under conditions comparable to those used in the production of both $C_6HF_5^-$ and $C_6F_6^-$, higher laser fluences were employed in order to observe any anion production (primarily to ensure that the gas mixture was indeed seeded with the $C_6H_2F_4$).

Prior to colliding with the ion detector, the mass-selected C₆HF₅ and C₆F₆ were photodetached using the second harmonic (532 nm, 2.330 eV) and third harmonic (355 nm, 3.495 eV) outputs of a Nd:YAG laser. The resulting photoelectrons were projected onto a 70 mm dual microchannel plate (MCP)/phosphor screen detector assembly with a velocity map imaging setup based on the design of Eppink and Parker, 46 situated perpendicular to the ion drift path. The images on the phosphor screen resulting from the MCPmultiplied electron signals were recorded using a CCD camera and the NuACQ 0.9 software provided by the Suits group.4 The three-dimensional velocity distributions were determined from the two-dimensional image using the BASEX program⁴⁸ and then converted to e KE, calibrated against the well-known PE spectrum of O₂^{-.49} The pBASEX code was used for image reconstructions, which are included in the Supporting Information, because it avoids centerline artifacts. 50

The e⁻KE is dependent on the detachment photon energy, hv. via

$$e^{-}KE = hv - EA - E_{int}^{neutral} + E_{int}^{anion}$$
 (1)

Where EA is the neutral electron affinity, $E_{\rm int}^{\rm neutral}$ is the internal (electronic, vibrational, rotational) energy of the neutral state(s) accessed via photodetachment, and $E_{\rm int}^{\rm anion}$ represents the internal energy of the anions. The instrumental resolution, $\Delta e^-KE/e^-KE$ is 2.5%. The spectra presented below are plotted against e^-BE , which is independent of the photon energy used:

$$e^{-}BE = hv - e^{-}KE \tag{2}$$

The e⁻BE values are the energies of the final neutral state(s) relative to those of the initial anion state.

2.2. Computational Details. The molecular structures of neutral and anionic substituted benzenes, hexafluorobenzene, pentafluorobenzene, 1,2,3,4-tetrafluorobenzene, 1,2,3,5-tetrafluorobenzene, and 1,2,4,5-tetrafluorobenzene, were calculated using the Gaussian 16 suite of electronic structure

calculations.⁵¹ The structures of each were optimized using DFT, specifically the Becke, 3-parameter, Lee-Yang-Parr (B3LYP)⁵² functional, and the aug-cc-pVTZ basis set. This method was selected because results are readily compared with those reported by Driver and Jena²⁹ on substituted benzenes, who aptly justified the method for determining the EAs of these species, pointing out that their results were in reasonable agreement with CCSD(T) for determining the (negative) EA of benzene.⁵³ We verified that minimum energy structures were determined for the doublet states of the anion and the singlet ground states and triplet excited states of the neutrals by ensuring no imaginary vibrational frequencies.

To directly compare the computational results with the experimental results, the EA of each neutral was computed as the difference between the zero-point-corrected energy of the optimized neutral and the corresponding optimized anion. Similarly, the adiabatic detachment energies (ADEs) associated with transitions to triplet excited states of the neutrals, which would be accessible via photodetachment of the doublet state of the anions given sufficient photon energy, were computed for pentafluorobenzene and hexafluorobenzene. The ADE value corresponds to the transition origin.

An additional point of comparison, particularly in the case of broad, vibrationally unresolved detachment bands (*vide infra*), is the VDE. This is the energy at which the vibronic manifold has maximum intensity due to the largest Franck—Condon overlap between the initial anion and final neutral state. The VDE is calculated as the difference between the electronic energy of the neutral confined to the optimized structure of the anion, and the electronic energy of the optimized anion.

For vibrationally resolved spectral transitions typical of similar anion and neutral geometries, we can use computed structures, vibrational modes, and vibrational frequencies to simulate the vibrational manifold of a detachment transition using home-written codes.⁵⁴ For broadened spectra with no resolved vibrational structure, simulating the spectra based on computed spectroscopic parameters is less informative. However, broadened manifolds consistent with ADE and VDE values can be used to graphically view the consistency between the computed structures and experimental data. For this study, we generated spectral simulations adhering strictly to the computed parameters. The simulations are done assuming a vibrational temperature of 300 K, and the simulated lines are convoluted with the e-KE-dependent experimental resolution. These thus-simulated bands are included in the Supporting Information.

3. RESULTS AND DISCUSSION

3.1. PE Spectrum of the Pentafluorobenzene Anion and Comparison to the Hexafluorobenzene Anion Spectrum. The PE spectrum of $C_6HF_5^-$ shown in Figure 1a obtained using both 3.495 eV photon energy (blue trace) and 2.330 eV photon energy (green trace) shows a broad transition, labeled X. The appearance of band X is due to extended and congested vibrational progressions and combination bands and indicates that the structure of the anion is significantly different from the known, planar C_{2v} structure of the neutral. Identification of the origin of the molecule is inherently difficult: the broadness of this transition raises the possibility that there is negligible intensity (i.e., negligible Franck—Condon overlap) at the origin. However, the onset of electron signal, defined here for consistency as at a level five times the baseline signal-to-noise level, is 0.53 ± 0.05 eV, and

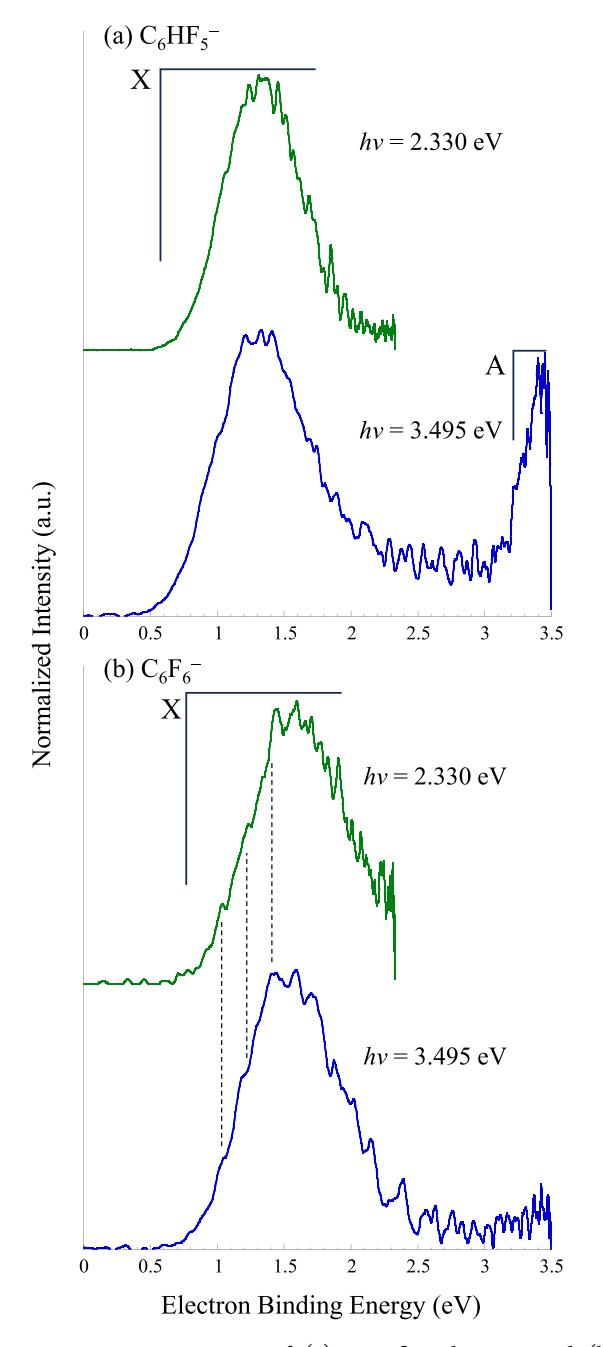


Figure 1. Anion PE spectra of (a) pentafluorobenzene and (b) hexafluorobenzene obtained using 2.330 (532 nm, green trace) and 3.495 eV (355 nm, blue trace).

the VDE is 1.33 ± 0.05 eV. These values are in fair agreement with our computed EA and VDE values, 0.43 and 1.45 eV, respectively. The computed and experimental EA and VDE values are summarized in Table 1.

We note that band X in the spectrum of $C_6HF_5^-$ obtained using 2.330 eV approaches baseline at e⁻BE > 2.2 eV, while in the spectrum obtained with 3.495 eV plateaus. While we do not have a firm explanation for this difference, this may be due to autodetachment from vibronic levels of excited states of the anion embedded in the detachment continuum and accessed with 3.495 eV photon energy. A similar effect was observed in other reported PE spectra of $C_6F_6^{-31,34}$

The PE spectrum of $C_6F_6^-$ shown in Figure 1b was measured previously in our group using a different instru-

Table 1. Results of Density Functional Theory Calculations On the ADE and VDE Values Calculated for Hexafluorobenzene, Pentafluorobenzene, and the Three Constitutional Isomers of Tetrafluorobenzene

molecule	calcd ¹ A - ² A EA/VDE (eV)	exp. ADE/VDE (eV)	calcd ³ A- ² A ADE (eV)	EA/VDE Davis et al. (eV) ^a	EA/VDE Driver and Jena $(eV)^b$
hexafluorobenzene	0.72/1.56	0.76(6)/1.60(5)	3.67	0.50/1.47	0.75/1.80
pentafluorobenzene	0.43/1.45	0.53(2)/1.33(5)	3.52	0.42/1.29	0.45/1.67
1,2,3,4- tetrafluorobenzene	0.13/0.98				
1,2,3,5- tetrafluorobenzene	0.004/0.63				0.01/1.22
1,2,4,5- tetrafluorobenzene	-0.10/-0.03			-0.17/0.28	

"Ref 37, using EOM-CCSD(T)(a)*. "Ref 29. "Experimental results from this study are included for comparison as well as computed results previously reported by Driver and Jena."

ment³³ and by others, ^{30-32,34} and is shown here for direct comparison with the spectrum of C₆HF₅⁻ obtained using the same instrument and under the same ion source conditions. The onset of electron signal in band X of our spectrum, which again approximates the EA, is 0.76 ± 0.05 eV, and the VDE is at 1.60 ± 0.05 eV. These values compare favorably to our computed values, 0.72 and 1.56 eV, respectively (Table 1), as well as the previously reported values. 30-34 While no fully resolved vibrational structure is observed in the spectrum, both the spectra obtained using 2.330 and 3.495 eV show a shoulder progression on the low e BE edge of the spectrum, indicated by dashed black lines which are spaced by 1520 cm⁻¹ (we do not ascribe an error to this spacing, since the shoulders could results from a convolution of progressions in several modes with similar frequencies). This value is close to the 1493 cm⁻¹ a_{1g} C-F stretch of C₆F₆. This partially resolved feature was not observed in previously reported spectra. 30-34

The PE spectra of C₆HF₅⁻ and C₆F₆⁻ are very similar in profile, with a modest difference in e⁻BE and ADE values. However, the spectrum of $C_6HF_5^-$ also exhibits a transition at the high-e⁻BE edge of the spectrum obtained using 3.495 eV, labeled "A." There are several potential explanations for band A. First, the transition from the doublet anion to the lowest lying triplet state of C₆HF₅ is computed to be 3.52 eV (Table 1) raising the possibility that band A is the low-e⁻BE edge of the transition to the triplet neutral. A second explanation is that the 3.495 eV photon could be resonant with an excited vibronic state (or manifold of vibronic states) of the $C_6HF_5^-$ anion, which could then undergo thermionic emission, 56,57 yielding electron signal at low e-KE (high e-BE). A third explanation is that the signal is due to the pentafluorophenide anion; the resolution of the mass spectrometer operating with settings necessary to generate sufficient ion signal to acquire the spectrum was not sufficient to fully separate m/z values of 167 and 168 (vide infra). The computed EA of the pentafluorophenyl radical (·C₆F₅) was reported elsewhere to be 3.22 eV, 58 which is in good agreement with the observed signal.

An analysis of the photoelectron angular distributions gleaned from the PE images eliminates one of these possible explanations. Plots of the PADs for bands X (solid blue circles) and A (gray diamonds) in the PE spectrum of $C_6HF_5^-$ obtained using 3.495 eV photon energy are shown in Figure 2a, and the same for band X (solid blue circles) in the PE spectrum of $C_6F_6^-$ is shown in Figure 2b. In addition, the PADs of band X obtained with 2.330 eV photon energy are included (open green circles) in both panels. To determine the PADs, slices through the reconstructed images at different

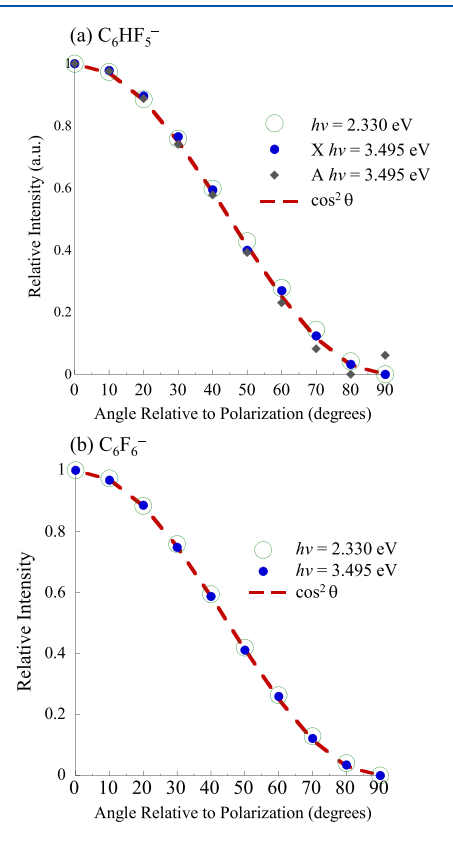


Figure 2. Integrated band intensities obtained from slices of reconstructed PE images as a function of angle relative to the electric field polarization vector of the detachment laser for (a) $C_6HF_5^-$ and (b) $C_6F_6^-$. Integrated intensities from PE images obtained using 2.330 eV photon energy are indicated by open green circles, those from PE images obtained using 3.495 eV photon energy are indicated by solid blue circles. In the case of (a) $C_6HF_5^-$, the high e⁻BE feature (A) observed in the 3.495 eV spectrum is indicated by gray diamonds. The red dashed curves in both panels is a $\cos 2\theta$ curve.

angles relative to the axis defined by the electric field vector of the laser were plotted (these plots are included in the Supporting Information), and the normalized integrals of the electronic transitions as a function of angle were determined graphically.

To interpret these PADs, we invoke Zare's expression of laboratory frame direct photodetachment, ⁵⁹

$$\frac{\mathrm{d}\sigma}{\mathrm{d}\Omega} = \frac{\sigma}{4\pi} \left[1 + \frac{\beta}{2} (3\cos^2\theta - 1) \right]$$

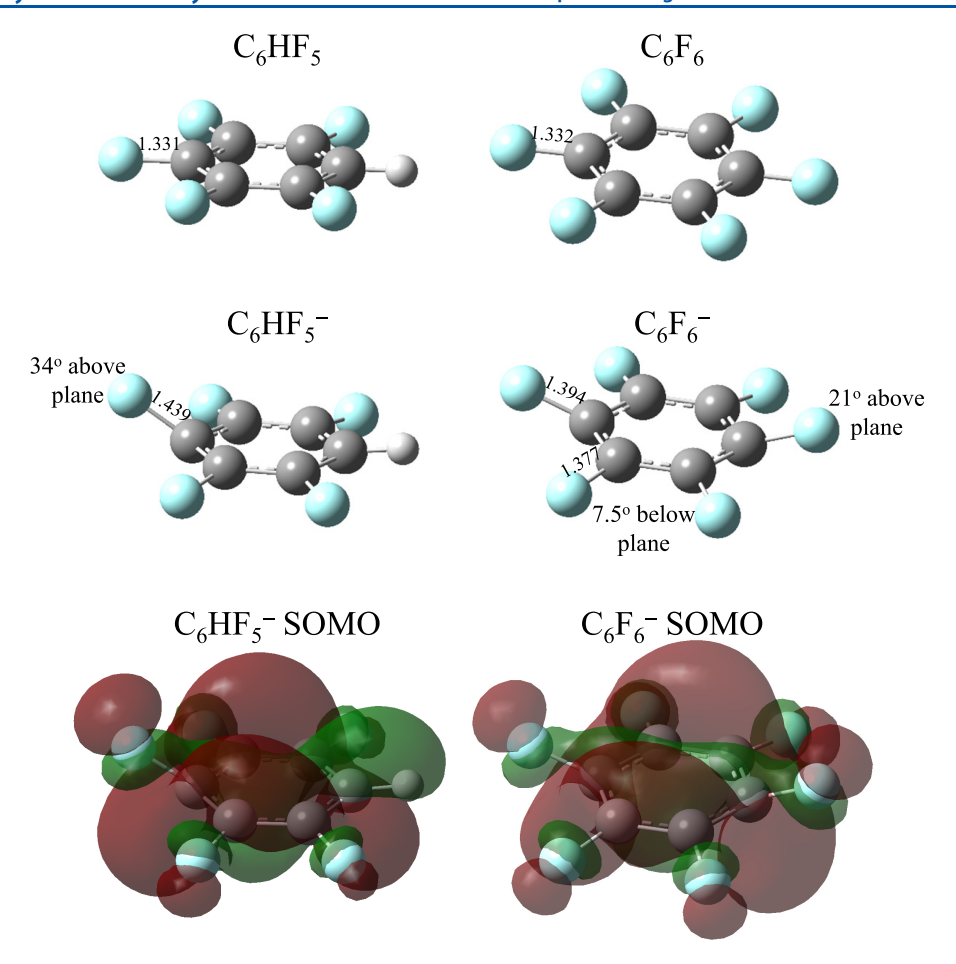


Figure 3. Molecular structures calculated for C_6HF_5 and C_6F_6 neutrals and anions, in addition to isosurfaces of the singly occupied molecular orbital (SOMO) of both anions (isovalue = 0.02). Details on all bond lengths and dihedral angles are included in the Supporting Information.

in which σ is the total photodetachment cross section, $\frac{\mathrm{d}\sigma}{\mathrm{d}\Omega}$ is the differential cross section with respect to the solid angle ($\mathrm{d}\Omega=\sin\theta\mathrm{d}\theta$), θ is the angle relative to the electric field vector of the laser, and β is the anisotropy parameter that can assume values between -1 and 2. The β value, in atomic systems, is governed by the symmetry of the orbital associated with the detachment and conservation of angular momentum. ^{60,61} For example, detachment from s-orbitals (l=0) yield photoelectrons with l=1 (p-wave), which would be have $\beta=2$, or parallel ($\cos^2\theta$) PADs.

In the case of the spectra of $C_6HF_5^-$ and $C_6F_6^-$, the PADs shown in Figures 2a,b follow a $\cos^2\theta$ curve, which is superimposed as a red dashed line on the plots. The detachment transition clearly yields p-wave photoelectrons. The PAD band A in the spectrum of $C_6HF_5^-$ rules out the possibility that it is due to thermionic emission, which would exhibit an isotropic PAD.

We now consider the molecular and electronic structures predicted by the calculations for a fuller analysis of the spectra. As noted above, the computed EA and VDE values are in good agreement with the observed broad spectra. The breadth and congestion of the transitions can be further understood from the molecular structures of the anion and neutral, shown in Figure 3. As expected, the neutral C_6HF_5 and C_6F_6 structures are predicted to be planar, with C_{2v} and D_{6h} symmetries, respectively. In contrast, the anions of both are nonplanar, with $C_6HF_5^-$ having C_s symmetry and $C_6F_6^-$ having C_{2v} symmetry.

Full details on the structures are included in the Supporting Information, but the main structural differences between the anion and neutral structures are shown in Figure 3. In C₆HF₅⁻, the C–F bond *para* to the C–H bond is predicted to be elongated by more than 0.1 Å relative to that of the neutral. The C₆ ring in the anion is nearly planar, but this unique C–F bond is bent 34° out of the plane. The remaining C–F bonds are bent 12° from the plane in the opposite direction. Other less significant structural differences include modest changes to all C–C bondlengths (some being longer in the anion, some being shorter) and the C–F bonds situated *ortho*- and *meta*-relative to the C–H bond (elongated by 0.04 Å relative to the neutral).

Similarly, the C_6 ring in $C_6F_6^-$ is nearly planar, with two C-F bond situated *para* to one another bent 21° out of the plane, with the remaining four C-F bonds bent 7.5° in the other direction. The C-F bonds are predicted to be 0.045–0.062 Å longer in the anion than the neutrals.

For both molecules, the structural differences would result in extended vibrational progressions in multiple out-of-plane bend modes, C-F stretch modes, and, to a lesser extent, ring distortion modes. The Supporting Information includes a full listing of all the neutral and anion vibrational frequencies and the calculated mass-weighted normal coordinate displacements, along with simulations based on the computed frequencies and normal coordinate displacements. The simulated spectra are broad and congested, though less broad than the observed transitions. This is likely due to a

limitation of our simulation codes, which make several assumptions that are not valid for large changes in structure upon photodetachment (normal modes, harmonic oscillator wave functions, parallel mode approximation) and potentially due to vibronic coupling. However, again, the computed VDEs are in very good agreement with the experimental spectra.

Reconciling PADs with detachment of polyatomic anions with lower symmetry has been detailed by Khuseynov et al. 62 and Sanov, 63 who invoked the Koopman's theorem approach and considered the atomic orbital contributions to the molecular orbital associated with the detachment transition. While we do not attempt to fully decompose the singly occupied molecular orbital (SOMO) of the two anions targeted in this study, the anions' SOMO isosurfaces (isovalue = 0.02) shown in Figure 3 can be qualitatively reconciled with the observed PADs. Despite both $C_6HF_5^-$ and $C_6F_6^-$ having symmetry lower than that of their neutral counterparts, their respective SOMOs both have significant C-F σ^* character, with the σ^* bonds radiating nearly symmetrically from the center of the molecule. The even s-like parity of these orbitals is consistent with the predominantly p-wave photoelectrons, i.e., parallel $(\cos^2\theta)$ PADs.

The question of the origin of band A in the PE spectrum can also be addressed here. The triplet neutral state would be accessed by detachment of an electron from the HOMO-1, a depiction of which is included in the Supporting Information. This orbital correlates with one component of the occupied degenerate π orbitals in benzene. We suggest that there would be differences in the PADs of transitions associated with these orbitals, which have different symmetries. On the other hand, the HOMO of pentafluorophenide is an in-plane orbital localized on what is the radical C center of the neutral, which is consistent with the observed PAD. Simulations of these two transitions are included in the Supporting Information and do not rule out either possible explanation. However, the computed EA of the pentafluorophenyl radical and the symmetry of the HOMO of the associated anion are more consistent with band A than the computed ADE for the transition to the triplet state of pentafluorobenzene and the symmetry of the MO associated with the transition.

3.2. Tetrafluorobenzene Anions are not Produced Using the Photoemission Ion source. The electron affinity of 1,2,3,5-tetrafluorobenzene was calculated to be 0.01 eV by Driver and Jena.²⁹ The least negative EA predicted by Davis et al. for 1,2,4,5-tetrafluorobenzene was -0.171 eV with EOM-CCSD(T) calculations.³⁷ Our own calculations on the three constitutional isomers of tetrafluorobenzene, summarized in Table 1, yielded comparable results, with 1,2,3,4-tetrafluorobenzene and 1,2,3,5-tetrafluorobenzene predicted to have positive EAs of 0.13 and 0.004 eV, respectively. 1,2,4,5-Tetrafluorobenzene has a predicted EA of -0.10 eV. Considering the DFT functional used in this study systematically overstabilizes higher spin states relative to lower spin states, 64 accounting for this systematic error by the typical 0.1 to 0.3 eV correction could result in a negative EAs for all three isomers.

Our inability to generate $C_6H_2F_4^-$ from any of the three constitutional isomers of tetrafluorobenzene seeded in the He carrier gas under the same source conditions as those used to produce $C_6HF_5^-$ and $C_6F_6^-$, while not definitive, is consistent with negative EAs for all constitutional isomers of $C_6H_2F_4$. Anions could only be generated with higher laser fluences in the photoemission source, which leads to molecular

fragmentation.³³ Mass spectra of anions generated from all three $C_6H_2F_4$ isomers, along with C_6HF_5 and C_6F_6 are shown in Figure 4. Figure 4a–c specifically shows the mass distributions from (a) 1,2,3,4-, (b) 1,2,3,5-, and (c) 1,2,4,5-tetrafluorobenzene. The m/z 150 position, which would be consistent with intact $C_6H_2F_4^-$, is highlighted by the red lines.

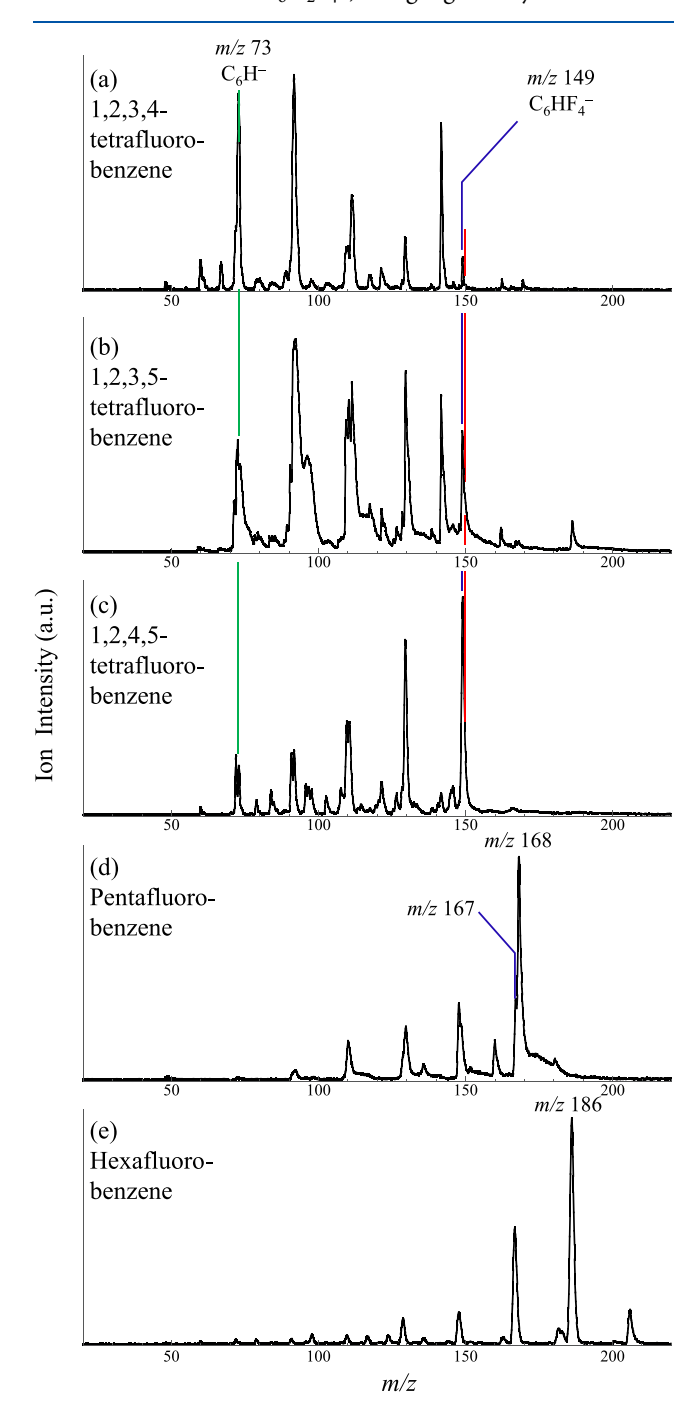


Figure 4. Mass spectra of anions generated from (a) 1,2,3,4-tetrafluorobenzene, (b) 1,2,3,5-tetrafluorobenzene, (c) 1,2,4,5-tetrafluorobenzene, (d) pentafluorobenzene, and (e) hexafluorobenzene. Ions with m/z values of 168 and 196 in panels (d) and (e) are consistent with intact $C_6HF_5^-$ and $C_6F_6^-$, respectively. The red vertical line corresponds to m/z 150, consistent with intact $C_6H_2F_4^-$, which is not observed. The anion of the tetrafluorophenide anion is observed at 1 unit below m/z 150. Panel (c) adapted with permission from ref 58. Copyright 2023 American Chemical Society.

Fragment anions include tetrafluorophenide (blue lines) and -F loss products down to $C_6H_x^-$. C_6H^- is indicated by the green line to show the full range of fluorine loss in all three cases. While a detailed analysis of the fragmentation and C-addition products is beyond the scope of this report, a full computational analysis of the fragmentation channels for this and other molecules in the $C_6H_{6-x}F_x$ series is in progress.

A series of fragment anions formed by F-loss are observed in the mass spectra from the pentafluorobenzene [Figure 4d] and hexafluorobenzene [Figure 4e] samples, with the intact $C_6HF_5^-$ and $C_6F_6^-$ ions dominating the respective mass spectra, further demonstrating that electron attachment to the intact molecules can be achieved with this ion source for species with positive EAs.

3.3. Evolution of Electronic Structures with F-Substitution. As the computational results are reasonably reconciled with the PE spectra $C_6HF_5^-$ and $C_6F_6^-$, as well as the absence of $C_6H_2F_2^-$, we look more deeply at the calculations to consider how the electronic structures of these neutrals and anions evolve with sequential fluorination and what features enable the binding of an electron. Experimentally, the difference in e⁻BE observed for $C_6F_6^-$ and $C_6HF_5^-$ is modest: the onset of electron detachment decreases from e⁻BE = 0.76 to 0.53 eV. This raises the question of why the decrease in fluorination from C_6HF_5 to $C_6H_2F_4$ is accompanied by a decrease in EA of more than 0.53 eV, considering that there are certainly electron-deficient $C_6H_2F_4$ isomers.

Fuhrer et al. recently described the evolution of the π systems in fluorinated benzenes. Each F-substitution on benzene is associated with an additional C-F π bonding orbital that lies energetically lower in energy than the other six π orbitals (including the C-F π^* orbital), the latter of which correlates closely to the six π orbitals of unsubstituted benzene. In forming a negative ion, the excess electron typically occupies the LUMO of the neutral precursor. In benzene, for example, the LUMO is the degenerate e_{2u} (π_4 , π_5) orbital. The lowest lying temporary anion of benzene is associated with the fleeting occupation of an electron in an e_{2u} , or π_4 , orbital (degeneracy also fleetingly broken). 2,3

With this in mind, we consider the LUMOs of neutral C_6F_6 , C_6HF_5 , and $C_6H_2F_4$ as well as the singly occupied MOs (SOMOs) of the respective anions. Figure 5 shows the SOMOS for the $C_6H_2F_4^-$ isomers along with the SOMOs of $C_6HF_5^-$ and $C_6F_6^-$ noted above and in Figure 3 but oriented for comparison with the other orbitals shown in Figure 5. The lowest unoccupied molecular orbital (LUMO) and the LUMO + 1 for the associated neutrals are also shown above the anion SOMOs on a relative energy scale (all relative to the neutral C_6F_6 LUMO).

We first consider the LUMO and LUMO + 1 of all neutral molecules in this study. What is immediately obvious is that the LUMO of neutral C_6F_6 does NOT correlate to the π_4 orbital of benzene (the neutral LUMO + 1 does). Rather, the LUMO can be described as the in-phase a_{1g} C-F σ^* orbital, which, because of the partial ionic character of the C-F bond, is predominantly sp² C orbitals, antibonding with respect to the less predominant F 2p orbitals. In contrast, the LUMOs of C_6HF_5 and the three constitutional isomers of $C_6H_2F_4$ do resemble the π_4 orbital (note that except for C_6F_6) the degeneracy of the π_4 and π_5 orbitals is broken, and only the

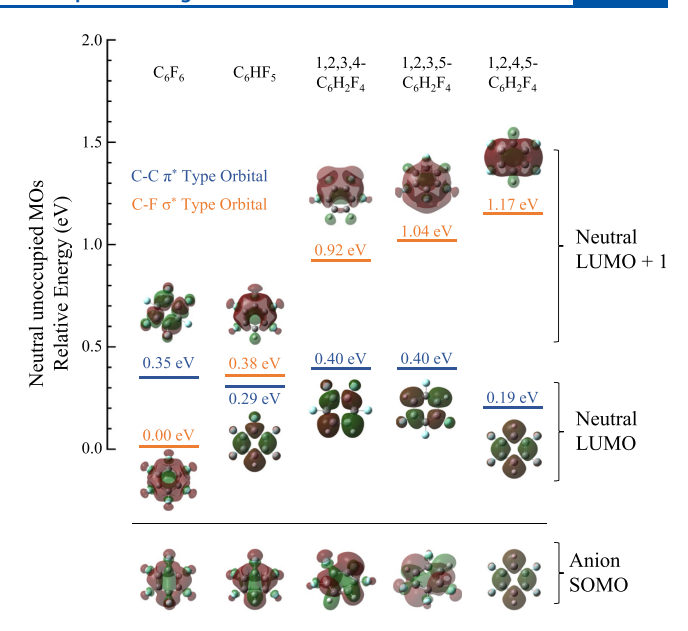


Figure 5. Depictions and relative energies of the two lowest energy unoccupied molecular orbitals (LUMO, LUMO + 1) the hexa-, penta-, and tetrafluorobenzenes included in this study. In the case of the π_3 and π_4 orbitals in both penta- and tetrafluorobenzene, these orbitals are not degenerate, and only one of the two orbitals correlating to the π_3 orbital in hexafluorobenzene is shown for simplicity. The π_4 orbital is close in energy in all cases.

lower energy of these two orbitals is shown here, for the sake of simplicity).

The neutral LUMO and LUMO+1 orbitals shown in Figure 5 are color coded to readily distinguish between the C–F σ^* orbitals (orange lines) and the π_4 orbitals (blue lines). The energy of the π_4 orbitals does not change significantly with fluorination, but the C–F σ^* orbitals are stabilized with fluorination. In neutral C₆HF₅, the π_4 -like LUMO is very close in energy to the C–F σ^* LUMO + 1 orbital, the latter of which is similar to the LUMO of C₆F₆, except that the C sp² "ring" is interrupted by the C–H bond. The C–F σ^* LUMO + 1 orbitals in neutral C₆H₂F₄ can be described in similar C–F σ^* terms. The energies of the LUMO + 1 orbitals in the three different constitutional isomers are similar, but the π_4 - σ^* gap is the largest for 1,2,4,5-tetrafluorobenzene.

We now reconsider the isosurfaces of the SOMOs computed for the anions of each species. As shown in Figures 3 and 5, both $C_6F_6^-$ and $C_6HF_5^-$ are predicted to have nonplanar structures, which indicates mixing of in-plane σ^* and out-of-plane π_4^* orbitals. The 1,2,3,4- and 1,2,3,5-tetrafluorobenzene anions also exhibit some π_4 - σ^* mixing, with modestly nonplanar structures. In contrast, the 1,2,4,5-tetrafluorobenzene anion is predicted to be planar, and consequently, the SOMO is identical to the LUMO of the neutral.

The computational results suggest the following: while the electron-withdrawing action of the -F substituents enables the most fluorinated benzenes to form stable anions, the stability of the anion is enhanced by delocalization of the excess charge in the SOMO. In C_6F_6 and C_6HF_5 , the excess charge is further stabilized by the low cost (energetically) of mixing the π_4 and σ^* orbitals enabled by distortion to a nonplanar structure, which results in an SOMO with less antibonding character. This orbital mixing is more energetically costly for tetrafluorobenzene because the σ^* is less delocalized around the ring, and therefore higher in energy. The (temporary) anion of

the isomer with the highest π_4 - σ^* energy interval remains planar. This isomer is calculated to have the most negative EA.

To summarize, the electron withdrawal from the C_6 ring and the availability of low-energy, delocalized LUMO and LUMO + 1 orbitals are both at play in the ability of F-substituted benzenes to form a valence-bound anion. A test of this inference would be mixed hexahalobenzenes, e.g., chloropentafluorobenzene, in which the difference between the C–F and C–Cl bonds could result in a changing energy interval between the C-X σ^* orbital and the π_4 orbital relative to hexafluorobenzene. These studies are currently underway.

On a final note, the inability to produce $C_6H_2F_4^-$ with the ion source used in this study does not definitively rule out a very small but positive EA for any of the constitutional isomers. A gentler ion production technique such as Rydberg electron transfer demonstrated by Bowen and co-workers, $^{66-68}$ may indeed provide a more definitive answer.

4. CONCLUSIONS

To measure the relationship between fluorine functionalization of benzene and EA, the new PE spectrum of the pentafluorobenzene anion was obtained compared to the hexafluorobenzene anion PE spectrum obtained under the same experimental conditions. Attempts to produce tetrafluorobenzene under identical conditions were unsuccessful, with the tetrafluorophenide anion produced under higherenergy ion source conditions.

An upper limit on the EA of pentafluorobenzene was determined to be 0.53 ± 0.05 eV based on the onset of electron signal observed in the PE spectrum, and the VDE was determined to be 1.33 ± 0.05 eV. The PE spectrum of hexafluorobenzene was in good agreement with previously published spectra. Further, DFT calculations presented here were in agreement with previously published calculations as well as the experimental PE spectra of both penta- and hexafluorobenzene anions. The calculations predict marginally positive EAs (0.004 eV and 0.013 eV) for two constitutional isomers of tetrafluorobenzene and a negative EA of -0.10 eV for the third. Taking into account the computational method's systematic overstabilization of higher spin states (i.e., the doublet anion) relative to lower spin states (i.e., the singlet neutral), the computational results are consistent with the inability to produce the tetrafluorobenzene anion.

Based on the calculations, the features of the electronic structures of these species and how they enable or disfavor the formation of a stable anion were considered. Calculations suggest that the LUMO of the hexafluorobenzene neutral is the in-phase C-F σ^* orbital, rather than the orbital correlating to the e_{2u} (π_4 , π_5 degenerate pair) LUMO of unsubstituted benzene. The C-F σ^* orbital has large contributions from the in-plane C sp³ orbitals and is delocalized symmetrically about the benzene ring. The comparable C-F σ^* orbital in pentafluorbenzene is interrupted at the C-H center but is still low-lying and is predicted to be energetically close to and just above the π_4 orbital. The C₆F₆ and C₆HF₅ anions are calculated to be nonplanar, and the SOMO of both anions are C-F σ^* - π_4 hybrid orbitals. For tetrafluorobenzene, the C-F σ^* is less delocalized and is significantly higher in energy than the π_4 orbital, increasing the cost of hybridization. Therefore, while tetrafluorobenzene has electron-deficient C-centers, the mechanism for stabilizing excess charge is energetically more costly in tetrafluorobenzene than in penta- and hexafluorobenzene.

ASSOCIATED CONTENT

Solution Supporting Information

The Supporting Information is available free of charge at https://pubs.acs.org/doi/10.1021/acs.jpca.3c04016.

Raw and reconstructed photoelectron images used in the measurement of the PE spectra, full computed structural parameters for the C_6F_6 and C_6HF_5 neutrals and anions, broad transition simulations of the PE spectra based computed ADE values, normal coordinate displacements, and vibrational frequencies, full list of vibrational frequencies of the C_6F_6 and C_6HF_6 neutral and anion frequencies, along with computed normal coordinate displacements between the anion and neutral structures, and plots of slices through the reconstructed $C_6HF_5^-$ and $C_6F_6^-$ PE images taken at different angles relative to the electric field polarization vector of the detachment laser (PDF)

AUTHOR INFORMATION

Corresponding Author

Caroline Chick Jarrold — Department of Chemistry, Indiana University, Bloomington, Indiana 47405, United States; orcid.org/0000-0001-9725-4581; Email: cjarrold@indiana.edu

Authors

Conor J. McGee – Department of Chemistry, Indiana University, Bloomington, Indiana 47405, United States Kristen Rose McGinnis – Department of Chemistry, Indiana University, Bloomington, Indiana 47405, United States

Complete contact information is available at: https://pubs.acs.org/10.1021/acs.jpca.3c04016

Notes

The authors declare no competing financial interest.

ACKNOWLEDGMENTS

The authors gratefully acknowledge support from the National Science Foundation under grant no. 2053889.

REFERENCES

- (1) Simons, J. Molecular Anions Perspective. J. Phys. Chem. A 2023, 127, 3940–3957.
- (2) Jordan, K. D.; Burrow, P. D. Temporary Anion States of Polyatomic Hydrocarbons. *Chem. Rev.* **1987**, *87*, 557–588.
- (3) Burrow, P. D.; Michejda, J. A.; Jordan, K. D. Electron Transmission Study of the Temporary Negative Ion States of Selected Benzenoid and Conjugated Aromatic Hydrocarbons. *J. Chem. Phys.* 1987, 86, 9–24.
- (4) Venuti, M.; Modelli, A. Low-Energy Electron Attachment to Fused 1,4-Cyclohexadiene Rings by Means of Electron Transmission Spectroscopy and Exponent Stabilization Calculations. *J. Chem. Phys.* **2000**, *113*, 2159–2167.
- (5) Pshenichnyuk, S. A.; Modelli, A. Electron Attachment to Antipyretics: Possible Implications of their Metabolic Pathways. *J. Chem. Phys.* **2012**, *136*, No. 234307.
- (6) Modelli, A.; Jones, D. Temporary Anion States and Dissociative Electron Attachment to Isothiocyanates. *J. Phys. Chem. A* **2006**, *110*, 13195–13201.
- (7) Csonka, I. P.; Szepes, L.; Modelli, A. Donor–Acceptor Properties of Isonitriles Studied by Photoelectron Spectroscopy and Electron Transmission Spectroscopy. *J. Mass Spectrom.* **2004**, *39*, 1456–1466.

- (8) Lyapustina, S. A.; Xu, S.; Niles, J. M.; Bowen, K. H. Solvent-Induced Stabilization of the Napthalene Anion by Water Molecules: A Negative Cluster Ion Photoelectron Spectroscopic Study. *J. Chem. Phys.* **2000**, *112*, 6643–6648.
- (9) Dobulis, M. A.; Thompson, M. C.; Sommerfeld, T.; Jarrold, C. C. Temporary Anion States of Fluorine Substituted Benzenes Probed by Charge Transfer in $O_2^- \cdot C_6 H_{6-x} F_x$ (x=0-5) Ion–Molecule Complexes. *J. Chem. Phys.* **2020**, *152*, No. 204309.
- (10) Kunin, A.; Neumark, D. M. Time-Resolved Radiation Chemistry: Femtosecond Photoelectron Spectroscopy of Electron Attachment and Photodissociation Dynamics in Iodide—Nucleobase Clusters. *Phys. Chem. Chem. Phys.* **2019**, 21, 7239—7255.
- (11) King, S. B.; Yandell, M. A.; Neumark, D. M. Time-Resolved Photoelectron Imaging of the Iodide—Thymine and Iodide—Uracil Binary Cluster Systems. *Faraday Discuss.* **2013**, *163*, 59–72.
- (12) Yandell, M. A.; King, S. B.; Neumark, D. M. Time-Resolved Radiation Chemistry: Photoelectron Imaging of Transient Negative Ions of Nucleobases. *J. Am. Chem. Soc.* **2013**, *135*, 2128–2131.
- (13) Stephansen, A. B.; King, S. B.; Yokoi, Y.; Minoshima, Y.; Li, W.-L.; Kunin, A.; Takayanagi, T.; Neumark, D. M. Dynamics of Dipoleand Valence Bound Anions in Iodide-Adenine Binary Complexes: A Time-Resolved Photoelectron Imaging and Quantum Mechanical Investigation. J. Chem. Phys. 2015, 143, No. 104308.
- (14) King, S. B.; Yandell, M. A.; Stephansen, A. B.; Neumark, D. M. Time-Resolved Radiation Chemistry: Dynamics of Electron Attachment to Uracil Following UV Excitation of Iodide-Uracil Complexes. *J. Chem. Phys.* **2014**, *141*, No. 224310.
- (15) Li, W.-L.; Kunin, A.; Matthews, E.; Yoshikawa, N.; Dessent, C. E.; Neumark, D. M. Photodissociation Dynamics of the Iodide-Uracil (I–U) Complex. *J. Chem. Phys.* **2016**, *145*, No. 044319.
- (16) Kunin, A.; Li, W.-L.; Neumark, D. M. Dynamics of Electron Attachment and Photodissociation in Iodide-Uracil-Water Clusters via Time-Resolved Photoelectron Imaging. *J. Chem. Phys.* **2018**, *149*, No. 084301.
- (17) Kunin, A.; McGraw, V. S.; Neumark, D. Time-Resolved Dynamics in Iodide-Uracil-Water Clusters upon Excitation of the Nucleobase. *J. Chem. Phys.* **2019**, *151*, No. 154304.
- (18) Xue, T.; Dixon, A. R.; Sanov, A. Anion Photoelectron Imaging Spectroscopy of Glyoxal. *Chem. Phys. Lett.* **2016**, *660*, 205–208.
- (19) Dauletyarov, Y.; Dixon, A. R.; Wallace, A. A.; Sanov, A. Electron Affinity and Excited States of Methylglyoxal. *J. Chem. Phys.* **2017**, *147*, No. 013934.
- (20) Dauletyarov, Y.; Wallace, A. A.; Blackstone, C. C.; Sanov, A. Photoelectron Spectroscopy of Biacetyl and Its Cluster Anions. *J. Phys. Chem. A* **2019**, *123*, 4158–4167.
- (21) Dobulis, M. A.; McGee, C. J.; Sommerfeld, T.; Jarrold, C. C. Autodetachment over Broad Photon Energy Ranges in the Anion Photoelectron Spectra of [O₂-M]⁻ (M = Glyoxal, Methylglyoxal, or Biacetyl) Complex Anions. *J. Phys. Chem. A* **2021**, *125*, 9128–9142.
- (22) Dobulis, M. A.; Thompson, M. C.; Jarrold, C. C. Identification of Isoprene Oxidation Reaction Products via Anion Photoelectron Spectroscopy. *J. Chem. Phys. A* **2021**, *125*, 10089–10102.
- (23) Chen, G.; Cooks, G. R. Electron Affinities of Polycyclic Aromatic Hydrocarbons Determined by the Kinetic Method. *J. Mass Spec.* **1995**, *30*, 1167–1173.
- (24) Kregel, S. J.; Thurston, G. K.; Garand, E. Photoelectron Spectroscopy of Anthracene and Fluoranthene Radical Anions. *J. Chem. Phys.* **2018**, 148, No. 234306.
- (25) Jalehdoost, A.; von Issendorff, B. Photon Energy Dependene of the Photoelectron Spectra of the Anthracene Anion: On the Influence of Autodetaching States. *J. Chem. Phys.* **2023**, *158*, No. 194302.
- (26) Mitsui, M.; Ando, N.; Nakajima, A. Mass Spectrometry and Photoelectron Spectroscopy of Tetracene Cluster Anions, (Tetracene)_n⁻ (n = 1–100): Evidence for the Highly Localized Nature of Polarizatino in a Cluster Analogue of Oligoacene Crystals. *J. Phys. Chem. A* **2007**, *111*, 9644–9648.
- (27) Sagan, C. R.; Anstöter, C. S.; Thodika, M.; Wilson, K. D.; Matsika, S.; Garand, E. Spectroscopy and Theoretical Modeling of

- Tetracene Anion Resonances. J. Phys. Chem. Lett. 2022, 13, 10245–10252.
- (28) Crocker, L.; Wang, T.; Kebarle, P. Electron Affinities of some Polycyclic Aromatic Hydrocarbons, Obtained from Electron-Transfer Equilibria. *J. Am. Chem. Soc.* **1993**, *115*, 7818–7822.
- (29) Driver, N.; Jena, P. Electron Affinity of Modified Benzene. *Int. J. Quantum Chem.* **2017**, *118*, No. e25504.
- (30) Eustis, S. N.; Wang, D.; Bowen, K. H.; Patwari, G. N. Photoelectron spectroscopy of hydrated hexafluorobenzene anions. *J. Chem. Phys.* **2007**, *127*, No. 114312.
- (31) Rogers, J. P.; Anstöter, C. S.; Bull, J. N.; Curchod, B. F. E.; Verlet, J. R. R. Photoelectron Spectroscopy of the Hexafluorobenzene Cluster Anions: $(C_6F_6)_n^-$ (n = 1–5) and I⁻ (C_6F_6) . J. Phys. Chem. A **2019**, 123, 1602–1612.
- (32) Nakajima, A.; Taguwa, T.; Hoshino, K.; Sugioka, T.; Naganuma, T.; Oho, F.; Watanabe, K.; Nakao, K.; Konishi, Y.; Kishi, R.; Kaya, K. Photoelectron Spectroscopy of $(C_6F_6)^-$ and $(Au-C_6F_6)^-$ Clusters. *Chem. Phys. Lett.* **1993**, 214, 22–26.
- (33) Williams, B. A.; Siedle, A. R.; Jarrold, C. C. Identification of Stable Perfluorocarbons Formed by Hyperthermal Decomposition of Graphite Fluoride Using Anion Photoelectron Spectroscopy. *J. Phys. Chem. C* **2022**, *126*, 9965–9978.
- (34) Rogers, J. P.; Anstoter, C. S.; Verlet, J. R. R. Ultrafast Dynamics of Low-Energy Electron Attachment via a Non-Valence Correlation-Bound State. *Nat. Chem.* **2018**, *10*, 341–356.
- (35) Voora, V. K.; Jordan, K. D. Nonvalence Correlation-Bound Anion State of C₆F₆: Doorway to Low-Energy Electron Capture. *J. Phys. Chem. A* **2014**, *118*, 7201–7205.
- (36) Wentworth, W. E.; Limero, T.; Chen, E. C. M. Electron Affinities of Hexafluorobenzene and Pentafluorobenzene. *J. Phys. Chem.* **1987**, *91*, 241–245.
- (37) Davis, J. U.; Jarrold, C. C.; Sommerfeld, T. Charge Distribution in Oxygen-Fluorobenzene Complex Anions $[O_2 \cdot C_6 H_{6-n} F_n]^-$ (n = 0 6). Chem. Phys. **2023**, 574, No. 112023.
- (38) Sherwood, C. R.; Garner, M. C.; Hanold, K. A.; Strong, K. M.; Continetti, R. E. Energy and Angular Distributions in Dissociative Photodetachment of O₄⁻. *J. Chem. Phys.* **1995**, *102*, 6949–6952.
- (39) Sherwood, C. R.; Hanold, K. A.; Garner, M. C.; Strong, K. M.; Continetti, R. E. Translational Spectroscopy Studies of the Photodissociation Dynamics of O₄⁻. *J. Chem. Phys.* **1996**, *105*, 10803–10811.
- (40) Patros, K. M.; Mann, J. E.; Jarrold, C. C. Photoelectron Imaging Spectra of O₂-·VOC and O₄-·VOC Complexes. *J. Phys. Chem. A* **2016**, 120, 7828–7838.
- (41) Posey, L. A.; Deluca, M. J.; Johnson, M. A. Demonstration of a Pulsed Photoelectron Spectrometer on Mass-Selected Negative Ions: O^- , O_2^- , and O_4^- . Chem. Phys. Lett. **1986**, 131, 170–174.
- (42) Hanold, K. A.; Continetti, R. E. Photoelectron-Photofragment Coincidence studies of the Dissociative Photodetachment of O₄⁻. *Chem. Phys.* **1998**, 239, 493–509.
- (43) Mann, J. E.; Troyer, M. E.; Jarrold, C. C. Photoelectron Imaging and Photodissociation of Ozonide in $O_3^-\cdot (O_2)_n$ (n = 1 4). *J. Chem. Phys.* **2015**, *142*, No. 124305.
- (44) Bakker, J. M. B. A Beam-Modulatd Time-of-Flight Mass Spectrometer. I. Theoretical Considerations. *J. Phys. E* **1973**, *6*, 785–789.
- (45) Bakker, J. M. B. Beam-Modulated Time-of-Flight Mass-Spectromber. 2. Experimental Work. J. Phys. E 1974, 7, 364–368.
- (46) Eppink, A. T. J. B.; Parker, D. H. Velocity Map Imaging of Ions and Electrons using Electrostatic Lenses: Application in Photoelectron and Photofragment Ion Imaging of Molecular Oxygen. *Rev. Sci. Instrum.* **1997**, *68*, 3477–3484.
- (47) Doyle, M. B.; Abeysekera, C.; Suits, A. G. NuAcq 0.9: Native Megapixel Ion Imaging with Centroiding to 4 Mpix Using Inexpensive USB-2 Cameras; Available at http://faculty.missouri.edu/suitsa/NuAqc.html.
- (48) Dribinski, V.; Ossadtchi, A.; Mandelshtam, V. A.; Reisler, H. Reconstruction of Abel-Transformable Images: The Gaussian Basis-

- Set Expansion Abel Transform Method. Rev. Sci. Instrum. 2002, 73, 2634–2642.
- (49) Ervin, K. M.; Anusiewicz, I.; Skurski, P.; Simons, J.; Lineberger, W. C. The Only Stable State of ${\rm O_2}^-$ is the ${\rm X^2\Pi_g}$ Ground State and It (Still!) Has an Adiabatic Electron Detachment Energy of 0.45 eV. *J. Phys. Chem. A* **2003**, *107*, 8521–8529.
- (50) Garcia, G. A.; Nahon, L.; Powis, I. Two-Dimensional Charged Particle Image Inversion Using a Polar Basis Function Expansion. *Rev. Sci. Instrum.* **2004**, *75*, 4989–4996.
- (51) Firsch, M. J.; Trucks, G. W.; Schlegel, H. B.; Scuseria, G. E.; Robb, M. A.; Cheeseman, J. R.; Scalmani, G.; Barone, V.; Mennucci, B.; Petersson, G. A. *GAUSSIAN 16*; Gaussian Inc.: Wallingford, CT, USA, 2016.
- (52) Becke, A. D. Density-Functional Exchange-Energy Approximation with Correct Asymptotic Behavior. *Phys. Rev. A* **1988**, 38, 3098–3100.
- (53) Hajgató, B.; Deleuze, M. S.; Tozer, D. J.; De Proft, F. A Benchmark Theoretical Study of the Electron Affinities of Benzene and Linear Acenes. *J. Chem. Phys.* **2008**, *129*, No. 084308.
- (54) Schaugaard, R. N.; Topolski, J. E.; Ray, M.; Raghavachari, K.; Jarrold, C. C. Insight into Ethylene Interactions with Molybdenum Suboxide Cluster Anions from Photoelectron Spectra of Chemifragments. *J. Chem. Phys.* **2018**, *148*, No. 054308.
- (55) Braden, D. A.; Hudson, B. S. C₆F₆ and sym-C₆F₃H₃: Ab Initio and DFT Studies of Structures, Vibrations, and Inelastic Neutron Scattering Spectra. *J. Phys. Chem. A* **2000**, *104*, 982–989.
- (56) Baguenard, B.; Pinare, J. C.; Lepine, F.; Bordas, C.; Broyer, M. Thermionic Emission in Small Carbon Cluster Anions. *Chem. Phys. Lett.* **2002**, 352, 147–153.
- (57) Horke, D. A.; Verlet, J. R. R. Photoelectron Spectroscopy of the Model GFP Chromophore Anion. *Phys. Chem. Chem. Phys.* **2012**, *14*, 8511–8515.
- (58) McGee, C. J.; McGinnis, K. R.; Jarrold, C. C. Trends in the Electron Affinities of Fluorophenyl Radicals, $C_6H_{5-x}F_x$ ($1 \le x \le 4$). *J. Phys. Chem. A* **2023**, *127*, 7264–7273.
- (59) Zare, R. N. Photoejection Dynamics [1]. Mol. Photochem. 1972, 4, 1–37.
- (60) Cooper, J.; Zare, R. N. Angular Distribution of Photoelectrons. *J. Chem. Phys.* **1968**, *48*, 942–943.
- (61) Cooper, J.; Zare, R. N. Erratum: Angular Distribution of Photoelectrons. J. Chem. Phys. 1968, 49, 4252.
- (62) Khuseynov, D.; Blackstone, C. C.; Culberson, L. M.; Sanov, A. Photoelectron Angular Distributions for States of any Mixed Character: An Experiment-Friendly Model for Atomic, Molecular, and Cluster Anions. *J. Chem. Phys.* **2014**, *141*, No. 124312.
- (63) Sanov, A. Laboratory-Frame Photoelectron Angular Distributions in Anion Photodetachment: Insight into Electronic Structure and Intermolecular Interactions. *Annu. Rev. Phys. Chem.* **2014**, *65*, 341–363.
- (64) Mayhall, N. J.; Rothgeb, D. W.; Hossain, E.; Raghavachari, K.; Jarrold, C. C. Electronic Structures of MoWO_y⁻ and MoWO_y Determined by Anion Photoelectron Spectroscopy and DFT Calculations. *J. Chem. Phys.* **2009**, *130*, No. 124313.
- (65) Fuhrer, T. J.; Houck, M.; Iacono, S. T. Fluoromaticity: The Molecular Orbital Contributions to Fluorine Substituents to the π -Systems of Aromatic Rings. *ACS Omega* **2021**, *6*, 32607–32617.
- (66) Liu, G.; Ciborowski, S. M.; Graham, J. D.; Buytendyk, A. M.; Bowen, K. H. Photoelectron Spectroscopic Study of Dipole-Bound and Valence-Bound Nitromethane Anions Formed by Rydberg Electron Transfer. *J. Chem. Phys.* **2020**, *153*, No. 044307.
- (67) Ciborowski, S. M.; Liu, G.; Graham, J. D.; Buytendyk, A. M.; Bowen, K. H. Dipole-Bound Anoins: Formed by Rydberg Electron Transfer (RET) and Studied by Velocity Map Imaging-Anion Photoelectron Spectroscopy (VMI-aPES). *Eur. Phys. J. D* **2018**, 72, 139.
- (68) Desfrancois, C.; Khelifa, N.; Lisfi, A.; Schermann, J. P.; Eaton, J. G.; Bowen, K. H. Electron Transfer Collisions Between Small Water Clusters and Laser-Excited Rydberg Atoms. *J. Chem. Phys.* **1991**, 95, 7760–7762.